Energy & Environmental Science

RSC Publishing

COMMUNICATION

View Article Online
View Journal | View Issue

A hybrid energy cell for self-powered water splitting†

Cite this: *Energy Environ. Sci.*, 2013, **6**, 2429

Ya Yang,[a] Hulin Zhang,[a] Zong-Hong Lin,[a] Yan Liu,[a] Jun Chen,[a] Ziyin Lin,[a] Yu Sheng Zhou,[a] Ching Ping Wong[a] and Zhong Lin Wang*[ab]

Received 30th April 2013
Accepted 30th May 2013

DOI: 10.1039/c3ee41485j

www.rsc.org/ees

Production of hydrogen (H_2) by splitting water using the electrolysis effect is a potential source of clean and renewable energy. However, it usually requires an external power source to drive the oxidation or reduction reactions of H_2O molecules, which largely limits the development of this technology. Here, we fabricated a hybrid energy cell that is an integration of a triboelectric nanogenerator, a thermoelectric cell, and a solar cell, which can be used to simultaneously/individually harvest mechanical, thermal, and/or solar energies. The power output of the hybrid energy cell can be directly used for splitting water without an external power source. The volume of the produced H_2 has a linear relationship with the splitting time at a production speed of 4×10^{-4} mL s^{-1}. Moreover, the produced energies can also be stored in a Li-ion battery for water splitting as well as other uses.

Broader context

We fabricated a hybrid energy cell that consists of a triboelectric nanogenerator, a thermoelectric cell, and a solar cell, which can be used to simultaneously or individually harvest the mechanical, thermal, and solar energies. Instead of using an external power source, the hybrid energy cell can be directly used for self-powered water splitting to generate hydrogen. The volume of the produced H_2 has a linear relationship with the splitting time at a production speed of 4×10^{-4} mL s^{-1}. Moreover, the produced energies can be stored in a Li-ion battery for water splitting and other uses.

Introduction

Hydrogen (H_2) as an environmentally benign fuel is one of the sustainable and clean-energies.[1] Currently, the main production of H_2 comes from steam reformation of natural gas, which not only consumes natural resources but also generates carbon dioxide as an undesired byproduct.[2] To be environmentally friendly and economically competitive, it is necessary to develop a cost-effective technology for mass production of H_2.[3] Photocatalytic splitting of water into H_2 and O_2 by using solar energy is one of the efficient approaches.[4,5] By using the electrolysis effect, water can be directly split into H_2, which was discovered more than 200 years ago.[6] However, an external power source for driving the oxidation or reduction reactions of H_2O molecules is mandatory for electrolysis, which makes it economically inefficient for energy applications. Alternatively, we may harvest energy from our living environment that can be directly utilized for electrolysis without using an external power source. The purpose of developing self-powered nanotechnology is to use the multimode energy sources for powering small electronic devices (such as LCDs, LEDs, and phones) or achieving some electrochemical applications (such as electrodeposition and electrodegradation).[7–9]

Harvesting mechanical, thermal, and solar energies is usually based on different physical effects. Utilizing the contact and separation between two polymers or polymer–metal materials, the triboelectric nanogenerators (TENGs) have been extensively designed for scavenging mechanical energy from irregular mechanical vibrations.[10,11] Thermal energy can be harvested using thermoelectric cells, which are based on the Seebeck effect.[12,13] Solar cells are usually fabricated using the optoelectronic effect.[14–16] However, these energies are not always available at the same time, depending on weather, day/night, and physical locations. Hybrid energy cells have been developed to simultaneously or individually harvest these energies by designing an integrated system,[17,18] which consists of three kinds of energy harvesters. In this paper, we demonstrated a hybrid energy cell that consists of a polyamide (PA)–perfluoroalkoxy (PFA) polymer film-based TENG, a Bi_2Te_3-based thermoelectric cell, and a silicon (Si)-based solar cell, which can be used to simultaneously/individually harvest mechanical,

[a]*School of Materials Science and Engineering, Georgia Institute of Technology, Atlanta, Georgia 30332-0245, USA. E-mail: zlwang@gatech.edu*

[b]*Beijing Institute of Nanoenergy and Nanosystems, Chinese Academy of Sciences, China*

† Electronic supplementary information (ESI) available: The additional movie files include the self-powered water splitting to generate H_2 by directly using the hybrid energy cell (movie file-1) and by using the charged Li-ion battery (movie file-2), where the playback speed of the movie was increased by 10 times than the normal speed. See DOI: 10.1039/c3ee41485j

thermal, and/or solar energies. Instead of the external power source, the power output from the hybrid energy cell was either directly used for water splitting to generate H_2 or charging Li-ion batteries.

Experimental

Fabrication of the hybrid energy cell

The fabricated TENG includes a PA film (thickness of 25 μm), a PFA film (thickness of 25 μm), and two Cu electrodes. A homemade force loading system was used to apply the periodically compressive forces on the TENG, where the contact/separation between the PA and PFA films can result in the output of the device. The bottom Bi_2Te_3-based thermoelectric cell was used to give the output voltage–current under the temperature difference across the device, which was induced by using a heated source. A temperature sensor was used to detect the change in temperature of the device.

For the Si-based solar cell, p-type silicon (100) wafers were used. KOH etching was performed in a solution of KOH (2–3 wt %), water, and isopropyl alcohol (20% by volume) at 80–85 °C for 20–30 min to create pyramidal structures. To form nanostructures, a thin discontinuous layer of Au nanoparticles was deposited by e-beam evaporation, followed by metal assisted chemical etching in a HF–H_2O_2 solution (49% HF, 30% H_2O_2, and H_2O with a volume ratio of 1 : 5 : 10) for 1 min. Subsequently, the Au nanoparticles were removed by immersing the samples in KI–I_2 (100 g of KI and 25 g of I_2 per 1 L of H_2O). The wafers were cleaned to remove surface organic and metallic contaminants, followed by $POCl_3$ diffusion to form the 65 Ω sq^{-1} n+-emitter. Al_2O_3 and SiN passivation layers were coated using Cambridge NanoTech Plasma ALD and Unaxis PECVD machines. After that Al paste and Ag grids were screen-printed on the backside and top of the Si substrate, followed by co-firing of both contacts. During the firing step, an Al-doped Si layer, referred to as the aluminum back surface field, is also formed. The silicon wafer was then cut into many pieces for the hybrid energy cells. Under the light illumination intensity of 100 mW cm^{-2}, the output performance of the solar cells was measured.

Measurement of the hybrid energy cell and the splitting of water to generate H_2

The output voltage of the device was measured using a low-noise voltage preamplifier (Keithley 6514 System Electrometer). The output current of the device was measured using a low-noise current preamplifier (Stanford Research SR560). The voltage–current curves of Si-based solar cells were measured by using a Keithley 4200 semiconductor characterization system. The performance of the Li-ion battery was measured using a battery analyzer (MTI Corporation). In the measurement of the splitting of water to generate H_2, the Pt electrode was used as the anode. 3% NaCl was added into the water solution to improve the conductivity. A transparent collection tube was used to store the produced H_2 at the cathode. A camera was used to record the time and the volume of the produced H_2.

Results and discussion

A schematic diagram of a fabricated hybrid energy cell is sketched in Fig. 1a. A TENG was fabricated on the top for harvesting mechanical energy. In this study, the PA and PFA polymer films at the opposite ends of the triboelectric series were purposely chosen as the triboelectric layers for the effective

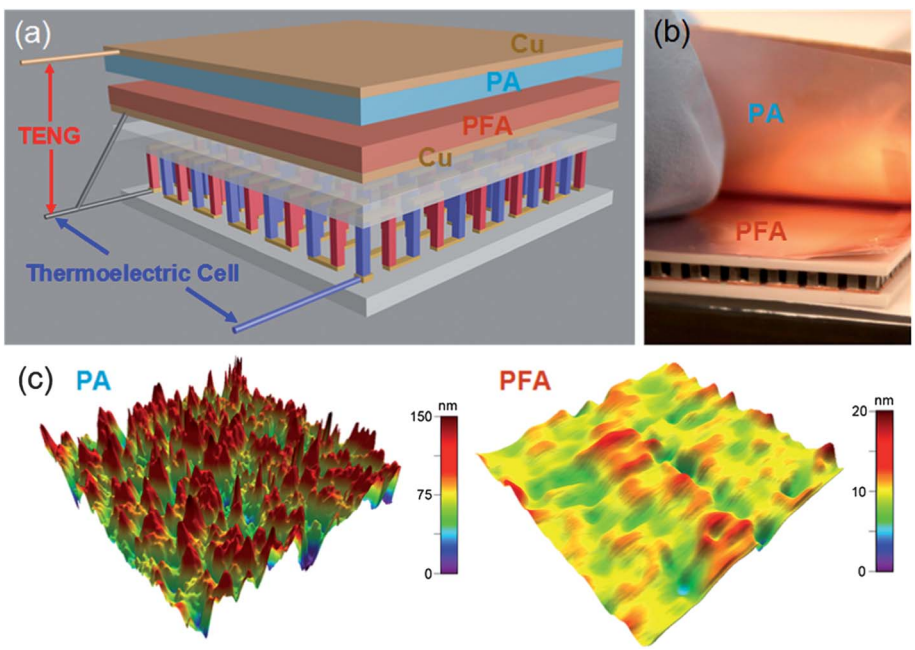

Fig. 1 (a) Schematic diagram of the fabricated hybrid energy cell including a TENG and a thermoelectric cell. (b) Photograph of the hybrid energy cell. (c) AFM images of the PA and PFA films.

electrification during the contact/separation process. On each polymer film, a layer of metal Cu electrode was fabricated on the external surface. A periodic loading force was applied on the top of the device to induce the contact and separation between the two polymer films. As illustrated in Fig. 1a, a Bi_2Te_3-based thermoelectric cell was designed at the bottom for harvesting thermal energy. A thermal source was used at the bottom of the device to create a temperature difference across the device. Fig. 1b shows the photograph of the fabricated device, where an Al_2O_3 layer with a thickness of 1 mm was placed between the thermoelectric cell and the TENG. Fig. 1c shows AFM images of the triboelectric PA and PFA films with an effective area of 30 μm × 30 μm. The surface of the PA film is rougher than that of the PFA film. The height of the aligned nanorod structures on the PA film surface is about 150 nm, which can enhance the triboelectric charge density on the surface.

Fig. 2a and b show the output performance of the fabricated TENG under the forward and reversed connections, respectively. The corresponding output voltage and current are about 110 V and 60 μA (the current density of 2.4 μA cm^{-2}), respectively. The mechanism of the TENG is based on the electron flow as driven by the triboelectric effect induced electrostatic charges on the surfaces of PA and PFA films. Because of the large difference in the ability to attract electrons, when the PA film is in contact with the PFA film, surface charge transfer takes place. Since PFA is much more triboelectrically negative than PA, electrons are injected from PA into the PFA surface, which can induce the electron flow in the external circuit and give the output signals.[19] The output voltage V_{oc} of TENG can be given by

$$V_{oc} = \frac{\sigma d}{\varepsilon_0} \quad (1)$$

where σ is the triboelectric charge density, d is the interlayer distance, and ε_0 is the permittivity in vacuum.[20] According to eqn (1), the output voltage V_{oc} can be increased by increasing the interlayer distance d.

Fig. 2c shows the output performance of the thermoelectric cell. For a temperature increase from 295 K at the top to 318 K at the bottom of the device, the largest output voltage and current of the device are about 2.2 V and 0.1 A, respectively. As compared with the TENG, the fabricated thermoelectric cell has a much smaller output voltage but much larger output current. Since the TENG gives alternating current (AC) output signals that do not match with the direct current (DC) output signals of the thermoelectric cell, a bridge rectification circuit was used to convert AC to DC signals. Fig. 2d shows the enlarged output voltage of the integrated hybrid energy cell, where the solar cell and the rectified TENG were connected in series. To clearly observe the small output voltage of the thermoelectric cell, the maximum output voltage was cut off at 15 V. The total output voltage of the hybrid energy cell is obviously larger than that of the thermoelectric cell. It can also be seen that the hybrid energy cell can simultaneously/individually harvest mechanical and thermal energies.

To illustrate the potential applications of the hybrid energy cell, we demonstrated that the energy produced by the hybrid cell can be directly used for splitting water into H_2. Fig. 3a shows a schematic diagram of the self-powered splitting of water into H_2 by using the electrolysis effect. There are two

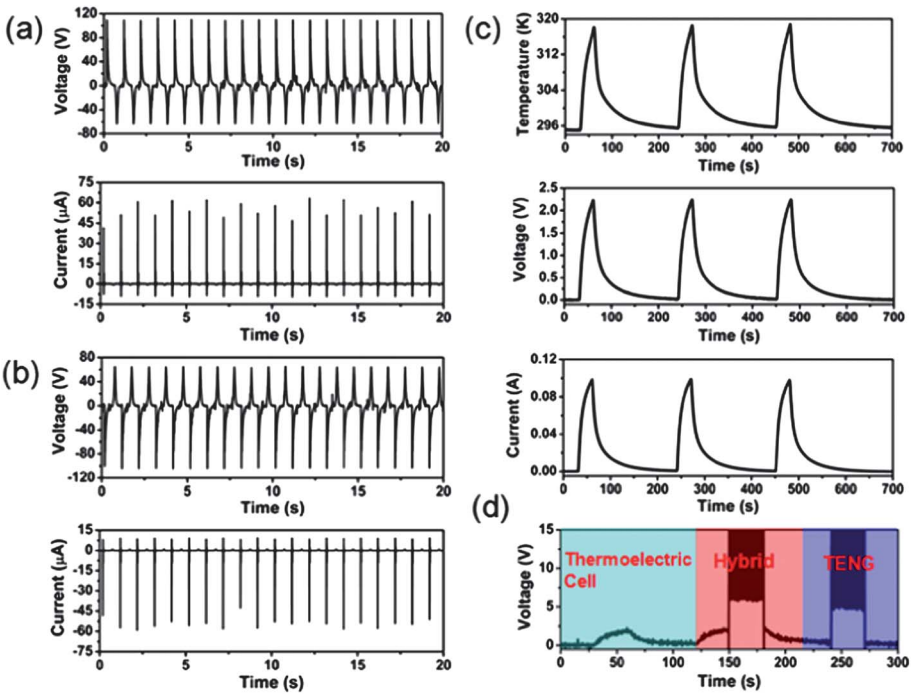

Fig. 2 (a and b) Output voltage and current of the fabricated TENG under the forward (a) and reversed (b) connections to the measurement system. (c) Change in temperature at the bottom of the thermoelectric cell, and output voltage and current of the thermoelectric cell. (d) Enlarged output voltage of the hybrid thermoelectric cell and TENG (after rectification) for harvesting thermal and mechanical energies.

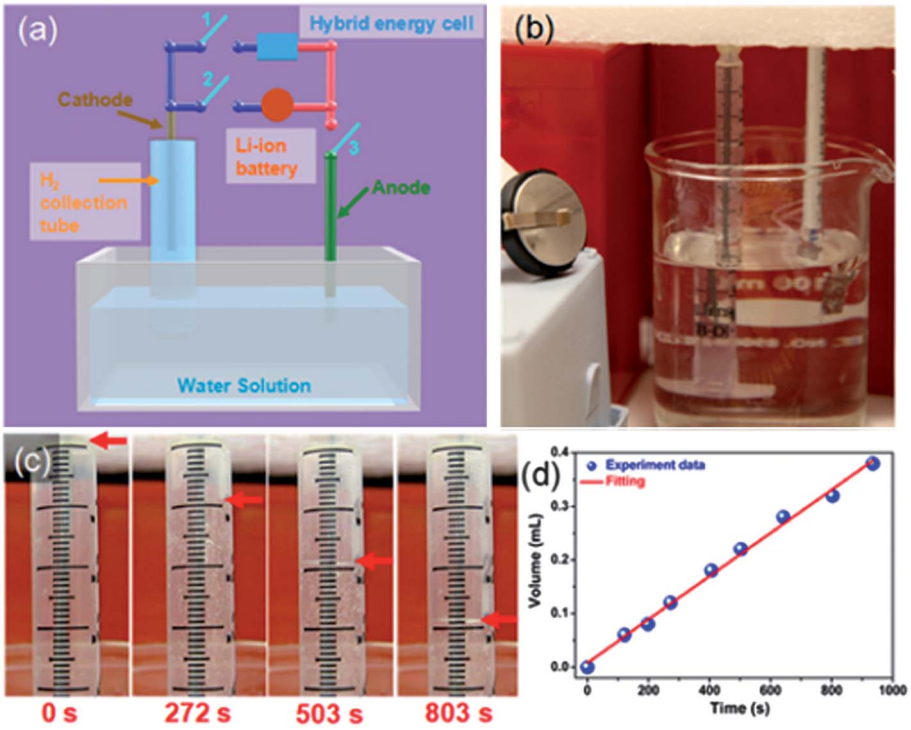

Fig. 3 (a) Schematic diagram of the system for self-powered splitting of water to generate H_2. (b) Optical image of the system for splitting of water into H_2. (c) Optical images of the H_2 collection tube under the different working times. (d) Corresponding volume of the produced H_2 under different working times.

methods to be used for water splitting. When the point "1" was connected to the point "3", the hybrid energy cell can be directly used for splitting of water, where the solar cell and the rectified TENG were connected in parallel. For the second method, when the point "1" was connected to the point "2", the produced energies can be stored in a Li-ion battery and then used for water splitting. In this study, a Pt electrode was used as the anode, which was put into a transparent container with the water solution. NaCl with a concentration of about 3% was added into water solution to improve the conductivity. The cathode was inserted into a H_2 collection tube and the top end of the tube was sealed by using epoxy. As shown in Fig. 3a, the H_2 collection tube was fully filled with water solution, and it was then partly inserted into the container, where the water solutions in the tube and the container were connected at the bottom of the tube. Due to the pressure of the atmosphere, the water solution cannot flow from the collected tube to the container. However, when the produced H_2 was collected on the top of the tube, the water solution can flow out from the collection tube due to the larger pressure of the produced H_2, resulting in the drop of water surface level in the tube.

According to the electrolysis effect,[6] the mechanism of water splitting is proposed as follows:

$$2NaCl \rightarrow 2Na^+ + Cl_2 + 2e^- \text{ (anode)} \quad (2)$$

$$2H_2O + 2e^- \rightarrow 2OH^- + H_2 \text{ (cathode)} \quad (3)$$

According to eqn (2) and (3), Cl^- was adsorbed to the anode for the oxidation reaction, resulting in the formation of Cl_2 at the anode. Moreover, the reduction of H_2O molecules occurs at the cathode, resulting in the production of H_2, which was collected in the tube. Fig. 3b shows a photograph of the fabricated self-powered water splitting system, where both the volume and the used time of the produced H_2 were recorded. Fig. 3c shows the optical images of the H_2 collection tube at different times, where the hybrid energy cell was directly used for water splitting. The volume of the obtained H_2 was found to dramatically increase with increasing time, resulting in the drop of water surface level in the collection tube. The dynamic splitting process of water into H_2 is also shown in movie file 1 in the ESI.† The change in volume of the produced H_2 at different times is plotted in Fig. 3d. The measured data show a linear relationship between the volume of H_2 and the elapsed time at a rate of 4×10^{-4} mL s^{-1}.

Usually, when two energy harvestors with the parallel connection give two different output voltages, the total output voltage of the hybrid device will approach the smaller one. Since the thermoelectric cell has a much smaller output voltage than that of the TENG, as shown in Fig. 2, it is necessary to increase the output voltage of the thermoelectric cell to match the output voltage of TENG. One method is that more thermoelectric cells can be connected to increase the total output voltage. However, in order to scavenge multimode energy by using the fabricated hybrid energy cell, we demonstrated that the Si-based solar cells can be used to harvest solar energy and increase the total output voltage of the devices in this study. A schematic diagram of the integrated hybrid energy cell is depicted in Fig. 4a, where the thermoelectric cell and the solar cell device were connected in series, and then they were connected with the rectified TENG in

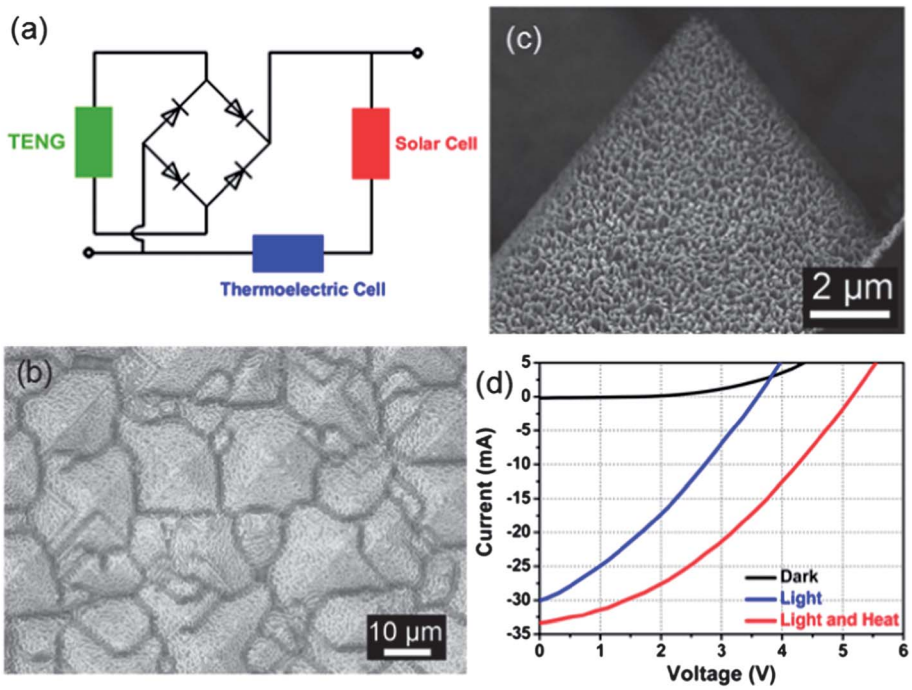

Fig. 4 (a) Schematic diagram of the hybrid energy cell. (b) SEM images of the fabricated micro-pyramid Si with the surface of nanoholes. (c) Cross-sectional SEM image of a single micro-pyramid. (d) Current–voltage characteristics of the hybrid energy cell under different conditions.

parallel. In a practical device, the fabricated solar cells can be attached on the top of the TENG, and it does not affect the output performance of the TENG. As a result, the top solar cells can harvest the solar energy, and the middle TENG can scavenge the mechanical energy. The bottom thermoelectric cells can convert thermal energy into electricity. The fabricated three kinds of energy harvesters can work at the same time. Moreover, the hybrid energy cell can ensure that there is always an output voltage–current when the mechanical, thermal, or solar energy is available.

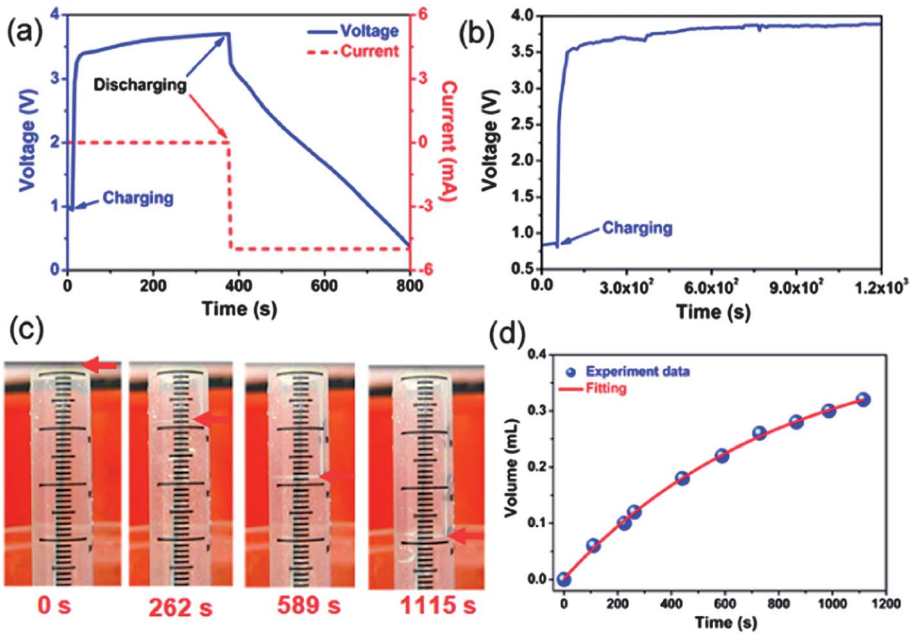

Fig. 5 (a) The hybrid mechanical, thermal, and solar energy cell-charging and the subsequent constant-current discharging curves of a Li-ion battery. (b) The charging curve of the Li-ion battery from 0.8 to 3.9 V. (c) Optical images of the H_2 collection tube under different working times for the splitting of water. (d) Corresponding volume of the produced H_2 under different splitting times.

Fig. 4b and c show the surface and cross-sectional SEM images of the fabricated pyramid Si solar cells, respectively. The sizes of the Si pyramids are smaller than 10 μm. To enhance the light absorption for improving the efficiency of the device, the surface of the micro-pyramid Si was etched into many nanoholes. The detailed fabrication method of the Si solar cell is given in the Experimental section. Under the light illumination intensity of 100 mW cm^{-2}, the open-circuit voltage of the device is about 0.62 V and the short-circuit current density is about 32 mA cm^{-2}, where the fill factor is about 80%. The energy conversion efficiency of the fabricated device is about 16%, which is much larger than that of the reported Si nanowire solar cells.[21] Fig. 4d shows the output performance of the integrated thermoelectric cell and the Si solar cells, which were connected in series. Under the light illumination, the output voltage of the hybrid energy cell is about 3.5 V and the output current is about 30 mA, which are due to the integration of 6 solar cells. Under the light illumination on the solar cells and the heat applied at the bottom of the thermoelectric cell, the total output voltage and current of these two energy harvestors were about 5.2 V and 34 mA, respectively.

For the second method of water splitting depicted in Fig. 3a, the energies produced by the hybrid energy cell were first stored in a Li-ion battery and then used for water splitting. Fig. 5a shows the charging and the subsequent constant current discharging curves of a Li-ion battery by using the hybrid energy cell. The Li-ion battery can be easily charged from 1 to 3.7 V in only about 376 s. Under a constant discharging current of 5 mA, the charged Li-ion battery can last for about 327 s before it gets back to the original value of 1 V, corresponding to a total electric capacity of 0.45 mA h. Fig. 5b shows that the same Li-ion battery can be charged from 0.8 to 3.9 V, which was used for splitting water to generate H_2. Fig. 5c shows the optical images of the H_2 collection tube under different splitting times by using the Li-ion battery. The volume of produced H_2 was found to obviously increase with increasing time, which is also shown in movie file 2 in the ESI.† By fitting the obtained data, the volume of the produced H_2 was found to have an exponential relationship with the splitting time, and the production speed of H_2 decreases with the increasing time, which is associated with the output power decrease of the Li-ion battery with the increasing discharging time.

Conclusions

In summary, we have developed the first hybrid energy cell that consists of a polymer film-based TENG, a Bi_2Te_3-based thermoelectric cell, and a Si-based solar cell, which can be used to simultaneously or individually harvest mechanical, thermal, and solar energies. The output power of the hybrid energy cell can be directly used for the splitting of water to generate H_2. The production volume of H_2 has a linear relationship with time, where the corresponding speed is about 4×10^{-4} mL s^{-1}. Moreover, the produced energies can also be stored in a Li-ion battery for the splitting of water into H_2 and other uses. The fabricated hybrid energy cells have potential applications for driving personal electronics (such as LCDs, LEDs, and phones) and achieving some electrochemical experiments (such as electrodeposition, pollutant degradation, corrosion protection, and water splitting).

Acknowledgements

This work was supported by Airforce, MURI, U.S. Department of Energy, Office of Basic Energy Sciences (DE-FG02-07ER46394), NSF, and the Knowledge Innovation Program of the Chinese Academy of Sciences (KJCX2-YW-M13).

Notes and references

1 J. H. Park, S. Kim and A. J. Bard, *Nano Lett.*, 2006, **6**, 24–28.
2 X. Yang, A. Wolcott, G. Wang, A. Sobo, R. C. Fitzmorris, F. Qian, J. Z. Zhang and Y. Li, *Nano Lett.*, 2009, **9**, 2331–2336.
3 N. S. Lewis, *Science*, 2007, **315**, 798–801.
4 Z. Liu, W. Hou, P. Pavaskar, M. Aykol and S. B. Cronin, *Nano Lett.*, 2011, **11**, 1111–1116.
5 E. Thimsen, F. L. Formal, M. Grätzel and S. C. Warren, *Nano Lett.*, 2011, **11**, 35–43.
6 K. Sun, Y. Jing, C. Li, X. Zhang, R. Aguinaldo, A. Kargar, K. Madsen, K. Banu, Y. Zhou, Y. Bando, Z. Liu and D. Wang, *Nanoscale*, 2012, **4**, 1515–1521.
7 Y. Yang, S. H. Wang, Y. Zhang and Z. L. Wang, *Nano Lett.*, 2012, **12**, 6408–6413.
8 Z. Guang, C. Pan, W. Guo, C.-Y. Chen, Y. Zhou, R. Yu and Z. L. Wang, *Nano Lett.*, 2012, **12**, 4960–4965.
9 Y. Yang, H. Zhang, S. Lee, D. Kim, W. Hwang and Z. L. Wang, *Nano Lett.*, 2013, **13**, 803–808.
10 F.-R. Fan, Z.-Q. Tian and Z. L. Wang, *Nano Energy*, 2012, **1**, 328–334.
11 X.-S. Zhang, M.-D. Han, R.-X. Wang, F.-Y. Zhu, Z.-H. Li, W. Wang and H.-X. Zhang, *Nano Lett.*, 2013, **13**, 1168–1172.
12 W. Liu, X. Yan, G. Chen and Z. Ren, *Nano Energy*, 2012, **1**, 42–56.
13 L. L. Baranowski, G. J. Snyder and E. S. Toberer, *Energy Environ. Sci.*, 2012, **5**, 9055–9067.
14 Q. Zhang, C. S. Dandeneau, X. Zhou and G. Cao, *Adv. Mater.*, 2009, **21**, 4087–4108.
15 J. Zhu, C.-M. Hsu, Z. Yu, S. Fan and Y. Cui, *Nano Lett.*, 2010, **10**, 1979–1984.
16 D. J. Lipomi, B. C.-K. Tee, M. Vosgueritchian and Z. Bao, *Adv. Mater.*, 2011, **23**, 1771–1775.
17 C. Xu, X. Wang and Z. L. Wang, *J. Am. Chem. Soc.*, 2009, **131**, 5866–5872.
18 C. Xu and Z. L. Wang, *Adv. Mater.*, 2011, **23**, 873–877.
19 J. A. Cross, *Electrostatics: Principles, Problems and Applications*, Adam Hilger, Bristol, 1987, ch. 2.
20 Y. Yang, L. Lin, Y. Zhang, Q. Jing, T.-C. Hou and Z. L. Wang, *ACS Nano*, 2012, **6**, 10378–10383.
21 C. Pan, Z. Luo, C. Xu, J. Luo, R. Liang, G. Zhu, W. Wu, W. Guo, X. Yan, J. Xu, Z. L. Wang and J. Zhu, *ACS Nano*, 2011, **5**, 6629–6636.

